

Simulation of thermal properties of proton-implanted top-surface-emitting lasers.

I. Analytical thermal model

WŁODZIMIERZ NAKWASKI

Institute of Physics, Technical University of Łódź, ul. Wólczajska 219, 93-005 Łódź, Poland.
Center for High Technology Materials, University of New Mexico, Albuquerque, NM, USA.

PAWEŁ MAĆKOWIAK

Institute of Physics, Technical University of Łódź, ul. Wólczajska 219, 93-005 Łódź, Poland.

MAREK OSIŃSKI

Center for High Technology Materials, University of New Mexico, Albuquerque, NM, USA.

A comprehensive analytical thermal model of proton-implanted top-surface-emitting lasers (PITSELS) is developed. In the model reasonable distributions of all important heat-generation mechanisms are taken into account, including nonradiative recombination, reabsorption of spontaneous radiation, free-carrier absorption of laser radiation as well as both volume and barrier Joule heating. Full self-consistency between the electrical and the thermal processes has been achieved including temperature dependences of thermal conductivities, threshold current, internal and external quantum efficiencies, voltage drop at the p-n junction, electrical resistivities and absorption coefficients.

1. Introduction

Vertical-cavity surface-emitting lasers (VCSELs) [1] have a number of unique features that distinguish them from conventional edge-emitting lasers (EELs) [2]. A typical list of those features would include inherent dynamic single-longitudinal-mode operation due to the short optical cavity length, presence of extremely high reflectivity mirrors necessary to compensate for the short length of the active medium, low-divergence circular nonastigmatic output beam, device geometry suitable for integration into two-dimensional (2D) arrays or for monolithic integration with electronic devices, compatibility with vertical-stacking architecture, and so on. However, the high-power continuous-wave (CW) performance of individual VCSELs as well as their integration scale in densely packed two-dimensional VCSEL arrays are still seriously limited by their thermal behaviour [2]. Complicated distribution of heat sources and 2D current- and heat-spread-

ing phenomena render the analysis of thermal problems in VCSELs difficult, which explains why there has been relatively little work [3]–[6] on this important subject.

Funneling of injected current through an aperture in a proton implanted region [7], [8] (or other ions [9]) is a very attractive technology for VCSEL manufacturing. The main advantages are: relative simplicity of fabrication with associated low cost [10], ability to increase the electrical resistivity of semiconductor layers located deeper than 1.0–1.5 μm under the surface while leaving the top material almost unaffected [11], practically unchanged refractive index that renders excitation of high-order transverse modes more difficult than in index-guided structures [12], practically unchanged thermal conductivity [13], and planar structure facilitating 2D heat removal from the active region.

Proton-implanted top-surface-emitting GaAs/AlGaAs lasers (PITSELs) have become the most popular VCSEL design, mostly because of their relatively simple technology, low series resistance [14], and wavelength compatibility (and associated cascading) with GaAs-based phototransistors and photothyristors [15]. Proton implantation is also used in modern GaAs/AlGaAs VCSELs [16]–[18], InGaAlP-based VCSELs [19], InGaAsP/InGaP/AlGaAs/AlAs VCSELs [20], InP/AlAs/GaAs VCSELs [21], InGaAlAs/InAlAs VCSELs [22] and even in proposed designs of nitride VCSELs [23].

We have already developed a comprehensive analytical self-consistent thermal-electrical model of etched-well double-heterostructure VCSELs with dielectric mirrors [3], [5]. This model, however, can not be used for PITSELs because from the thermal point of view their structures are completely different. The PITSEL thermal analysis requires development of an entirely new and mathematically more advanced model.

In this paper, a comprehensive, analytical, two-dimensional thermal model of PITSEL is described in which all important features of a PITSEL design are successfully taken into consideration. The model is based on an advanced analytical thermal approach that features realistic distributions of heat sources combined with 3D treatment of heat-flux spreading. In the analysis, all important heat-generation mechanisms are taken into account, including nonradiative recombination, re-absorption of spontaneous radiation, free-carrier absorption of laser radiation as well as volume and barrier Joule heating. Full self-consistency between the electrical and thermal processes has been achieved including temperature dependences of thermal conductivities, threshold current, internal and external quantum efficiencies, voltage drop at the p-n junction, electrical resistivities and absorption coefficients. In the first part of the paper, the self-consistent thermal-electrical PITSEL model is presented. Its results are discussed in the second part of the paper [24].

In successive sections of the present paper, the laser structure under consideration is described (Sec. 2), the heat sources are analysed (Sec. 3), analytical formulation of the PITSEL thermal model is presented (Sec. 4), solution algorithm is given (Sec. 5) and model convergence (Sec. 6) and model self-consistency (Sec. 7) are discussed, which is followed by conclusions (Sec. 8).

2. Laser structure

Figure 1 shows a schematic view of a GaAs/AlGaAs/AlAs PITSEL. For simplicity, the device is assumed to be cylindrically symmetric. The specific device structure under consideration is similar to the first historical VCSEL design for which the room-temperature continuous-wave operation was reported [25]. This design remains still a typical PITSEL construction. The graded-index separate-confine-

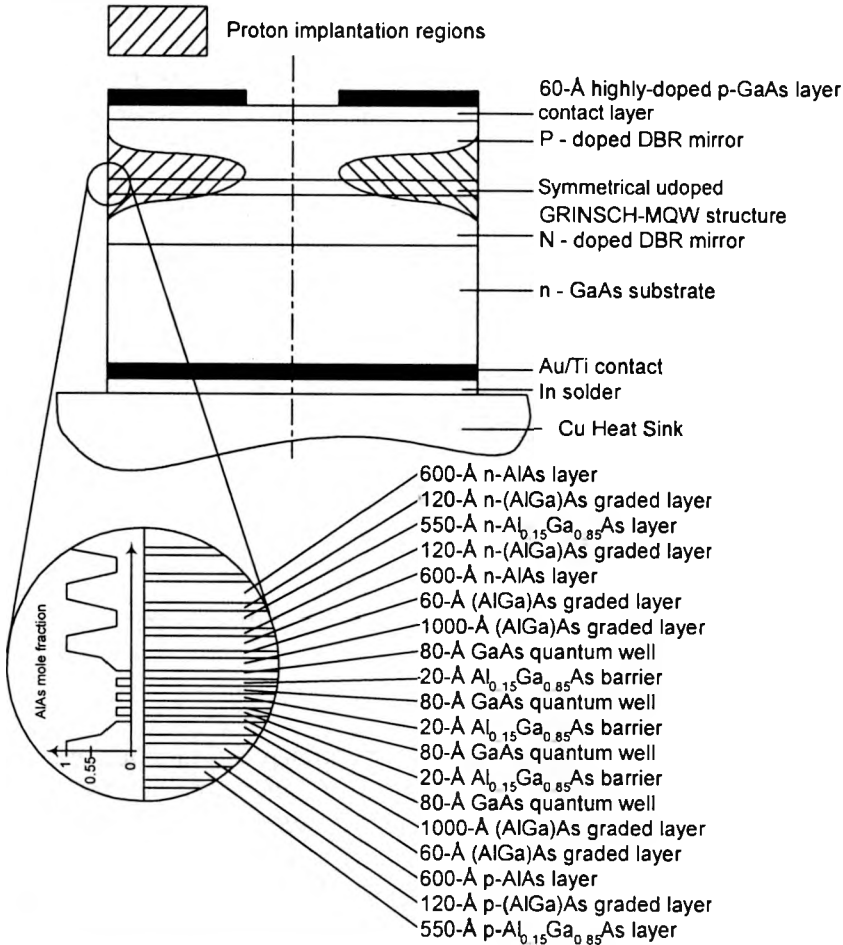


Fig. 1. Schematic structure of a photon-implanted top-surface-emitting GaAs/AlGaAs/AlAs vertical cavity semiconductor laser (PITSEL) mounted p-side up. Active region neighbourhood is enlarged.

ment-heterostructure (GRINSCH) active region consists of several GaAs/AlGaAs-quantum wells and is sandwiched between two multilayer AlGaAs/AlAs Bragg reflectors. Lateral boundaries of the active region are defined by highly resistive

proton-implanted regions. The device is mounted p-side up. In order to reduce series electrical resistance, all interfaces in the distributed-Bragg-reflector (DBR) sections are linearly graded. In addition, the p-contact layer is very highly doped, facilitating the radial current spreading.

3. Heat sources

Thermal analysis of the top-surface-emitting VCSELs is performed using a self-consistent model that features realistic distribution of heat sources combined with three-dimensional treatment of heat-flux spreading. Three main heat sources are considered: active region (nonradiative recombination, reabsorption of spontaneous radiation, free-carrier absorption of laser radiation and Joule heating in the GRINSCH structure), P-type Bragg mirror (free-carrier absorption and Joule heating, including the heterobarriers), and the N-type Bragg mirrors (as the above).

3.1. Nonradiative recombination and reabsorption of spontaneous radiation

This heat source is located within the active region. Its heat density $q_A(T)$, where T is temperature, can be expressed by a modified version of Eq. (15) from [3]

$$q_A(r, T) = U(r, T) \{j_{th}(r, T) + [j(r) - j_{th}(r, T)][1 - \eta_{int}(T)]\}, \quad [\text{Wcm}^{-2}] \quad (1)$$

where j_{th} , j , U and η_{int} are the CW threshold current density, the operation current density, the voltage drop at the p-n junction and the internal quantum efficiency, respectively. Temperature dependences of these parameters will be discussed in [24]. Relative radial changes of the threshold current density are assumed identical with those of the operation current density.

3.2. Absorption of laser radiation

Heat generation associated with the absorption of laser radiation within the i -th layer is described by

$$q_{abs,i}(T) = P_{int}(T) \alpha_i(T) d_i, \quad [\text{Wcm}^{-2}] \quad (2)$$

where $\alpha_i(T)$ is the absorption coefficient of the i -th layer material (mainly accounting for free-carrier absorption), d_i is the thickness of the i -th layer under consideration, and $P_{int}(T)$ is the internal radiation density, *i.e.*, the density of radiation inside the resonator

$$P_{int}(T) = U(T) \eta_d(T) [j - j_{th}(T)] (1 + \xi) \frac{1 + R_T}{1 - R_T}, \quad [\text{Wcm}^{-2}]. \quad (3)$$

In Equation (3), $\eta_d(T)$ is the external differential quantum efficiency, R_T is the reflection coefficient of the top Bragg reflector, and ξ is a parameter taking into account emission of radiation through the bottom mirror, given by [26]

$$\xi = \frac{(1 - R_B) R_T^{1/2}}{(1 - R_T) R_B^{1/2}} \quad (4)$$

with R_B standing for the reflection coefficient of the bottom reflector.

For the n-type and the p-type GaAs, respectively, the free-carrier absorption coefficients at room-temperature (RT) are given by [27]

$$\alpha_{fc,n}(300 \text{ K}) = 3 \times 10^{-18} n, \quad [\text{cm}^{-1}], \quad (5a)$$

$$\alpha_{fc,p}(300 \text{ K}) = \exp[2.856(10^{-18} p)^{0.1723}], \quad [\text{cm}^{-1}] \quad (5b)$$

where the free-carrier concentrations n and p are expressed in cm^{-3} . For AlAs and $\text{Al}_x\text{Ga}_{1-x}\text{As}$, *i.e.*, the wider-bandgap materials, the above relations should be very similar which has been confirmed by observations reported in [28]–[30]. Therefore, we assume identical expressions (5a) and (5b) for all $\text{Al}_x\text{Ga}_{1-x}\text{As}$ materials, disregarding their composition x .

On the basis of measurements reported in [31], the temperature dependence of free-carrier absorption is assumed to be given by

$$\alpha_{fc,n(p)}(300 \text{ K} + \Delta T) = \alpha_{fc,n(p)}(300 \text{ K})(1 + 1.28 \times 10^{-3} \Delta T), \quad [\text{cm}^{-1}] \quad (6)$$

where ΔT the temperature increase.

For the Si-doped n-type $\text{Al}_x\text{Ga}_{1-x}\text{As}$, the free-carrier concentration n is determined using the activation energy vs. composition relation given in [32], whereas for the C-doped p-type $\text{Al}_x\text{Ga}_{1-x}\text{As}$, a constant value of its activation energy, $E_A = 30 \text{ meV}$, is assumed disregarding its composition, on the basis of experimental results reported in [33].

In the undoped active region, bimolecular recombination is assumed. The free-carrier concentrations in this region, n_A and p_A , may be determined from the actual value of the threshold current density j_{th}

$$n_A = p_A = \left(\frac{j_{th}}{B e d_A} \right)^{1/2} \quad (7)$$

where $d_A = N_{QW} d_{QW}$ is the cumulative thickness of the active region, N_{QW} is the number of the active-region quantum wells, d_{QW} is the thickness of each of these identical quantum wells, e is the electron charge, and B is the radiative recombination coefficient ($B = 10^{-10} \text{ cm}^3/\text{s}$ [34]). Note that the free-carrier absorption in the active region is associated with both electrons and holes.

3.3. Volume Joule heating

The density of the Joule heating in the i -th layer is given by the following formula:

$$q_{J,i}(r, T) = j^2(r, T) \rho_i(T) d_i, \quad [\text{Wcm}^{-2}] \quad (8)$$

where ρ_i stands for the electrical resistivity (in Ωcm) of the i -th-layer material. For each layer, its value at a given temperature is determined taking into account the temperature dependence of the carrier concentration (discussed already in Sec. 3.2) and the mobility-temperature relation extracted from numerous experimental data (*cf.* [24]).

3.4. Heterobarrier Joule heating

For an ideal laser structures, its series electrical resistance $R_{s,id}$ is determined from known values of electrical resistivities and thicknesses of all the layers, using the

approach reported in [35]. The residual barrier electrical resistance is then found from the measured value of resistance as a surplus over $R_{s, id}$. We assume that 80% of the heterobarrier resistance is associated with the p-type DBR mirror, and 20% – with the n-type DBR mirror.

4. Analytical formulation of thermal model of PITSEL's

The thermal model of the PITSEL structure is shown schematically in Fig. 2. We assume the axial symmetry of the mathematical problem considered here

$$\left. \frac{\partial T}{\partial r} \right|_{r=0} = 0, \quad (9)$$

so we can use the cylindrical coordinate system, and effectively solve the two-dimensional heat conduction equation by neglecting the azimuthal dependence

$$\nabla \{k[r, z, T(r, z)] \nabla T(r, z)\} = -g[r, z, T(r, z)] \quad (10)$$

where k is the thermal conductivity (in W/cmK) and g is the heat source density distribution (in W/cm³). As indicated in Eq. (10), nonuniformities of both the structure (*i.e.*, different thermal conductivities of different materials) and the heat generation process are taken into account. Also temperature dependences of k and g are considered.

The heat extraction by the side and top walls of the laser chip, due to thermal radiation and acceptance of thermal energy from the chip surface by air particles, is assumed to be negligible in comparison with highly effective heat transmission process from the laser volume through the bottom contact to the heat sink. Corresponding boundary conditions are:

$$\left. \frac{\partial T}{\partial r} \right|_{r=r_S} = 0, \quad (11a)$$

$$\left. \frac{\partial T}{\partial z} \right|_{z=z_N} = 0 \quad (11b)$$

where $r_S = D_S/2$ is the radius of the laser chip and z_N is the z -coordinate of its top surface (see Fig. 2).

We assume the heat capacity of the heat sink to be infinite because of its relatively large dimensions in comparison with the laser chip as well as because the thermal conductivity of the heat sink material is much higher than that of semiconductor layers, therefore

$$T(z = 0) = T_A + \Delta T_{HS} \quad (12)$$

where T_A is the ambient temperature and ΔT_{HS} is the temperature increase within the heat sink, discussed in Sec. 4 of [24].

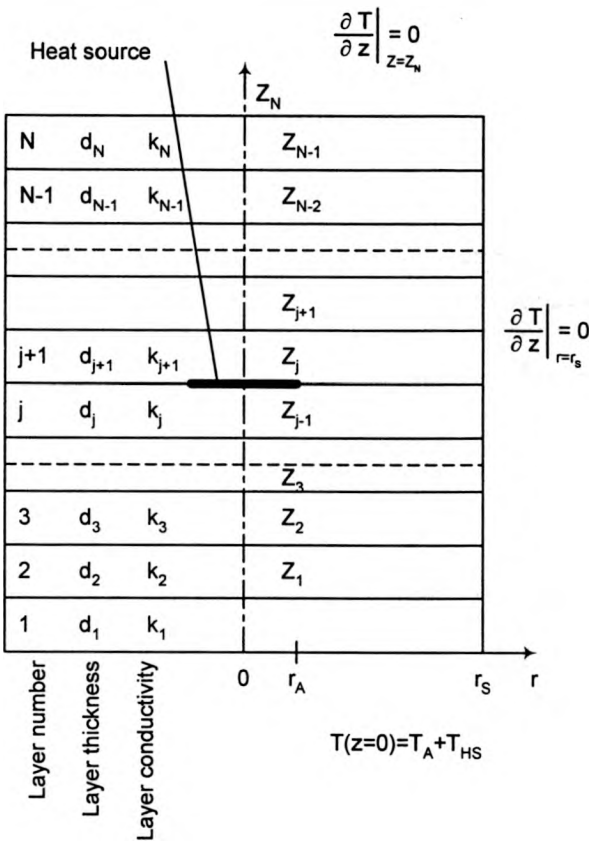


Fig. 2. Schematic view of the thermal model of PITSEL.

Each of the heat sources analysed in Sec. 3 is assumed to be located in the mid-plane of the corresponding region. An analytical solution is obtained for the entire structure separately for each heat source. Using the superposition principle, a cumulative temperature distribution in the whole volume of the device is determined by adding together contributions from all heat sources. Subsequently, a self-consistent solution is found with the aid of an iteration procedure, taking into account the temperature dependences of device parameters, including thermal conductivities, threshold current, electrical resistivities, voltage drop at the p-n junction, free-carrier absorption as well as internal and external differential quantum efficiencies. The flow chart of numerical calculations is illustrated in Fig. 3. Note that large temperature variations in VCSELs affect substantially their lasing characteristics, because of strongly nonlinear thermal-electrical interactions, eventually leading to thermal runaway.

For each flat heat source situated between the j -th and the $(j+1)$ -th layers (see Fig. 2) and for each i -th layer, we are solving for the two-dimensional temperature distribution in the following form:

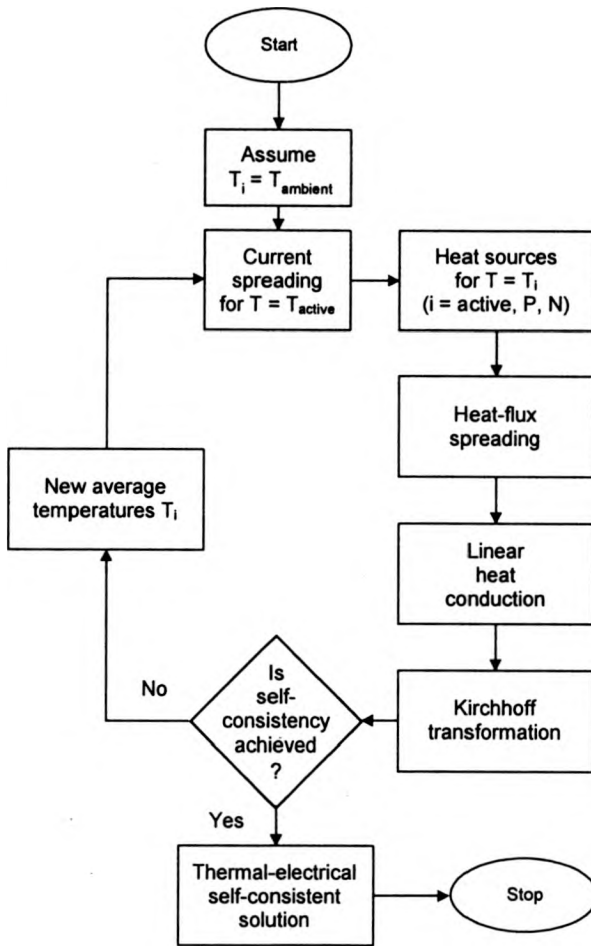


Fig. 3. Flow chart of the self-consistent thermal-electrical model of PITSELS.

$$T_{j,i}(r, z) = T_A + \Delta T_{HS} + \alpha_{j,i,0} + \beta_{j,i,0}(z - z_{i-1}) + \sum_{n=0}^{\infty} \{ \alpha_{j,i,n} \cosh [\kappa_n(z - z_{i-1})] + \beta_{j,i,n} \sinh [\kappa_n(z - z_{i-1})] \} \frac{J_0(\kappa_n r)}{J_0^2(\kappa_n r_S)} \quad (13)$$

where $z_{i-1} \leq z \leq z_i$ and κ_n are successive roots of the equation

$$J_1(\kappa_n r_S) = 0, \quad (14)$$

J_0 and J_1 are the zero-order and the first-order Bessel functions of the first kind, while $\alpha_{j,i,n}$ and $\beta_{j,i,n}$ are the coefficients to be determined in Sec. 5.

Solution of Eq. (10) may be expressed in the form (13) because, for roots fulfilling the condition (14), functions $J_0(\kappa_n r)$ form an orthogonal r -weighted system of functions in the interval $r \in [0, r_S]$. Then any given function $Q(r)$, defined in the above

interval and fulfilling the Dirichlet condition, may be represented in the following way [36]:

$$Q(r) = C_0 + \sum_{n=1}^{\infty} C_n J_0(\kappa_n r) \quad (15)$$

with

$$C_0 = \frac{2}{r_s^2} \int_0^{r_s} Q(r) r dr, \quad (16a)$$

$$C_n = \frac{2}{[r_s J_0(\kappa_n r_s)]^2} \int_0^{r_s} Q(r) J_0(\kappa_n r) r dr. \quad (16b)$$

In particular, for a uniform heat source of the form

$$Q_u(r) = \begin{cases} q_j & \text{for } 0 \leq r \leq r_A \\ 0 & \text{for } r_A \leq r \leq r_s \end{cases} \quad (17)$$

the above relations reduce to the following expressions:

$$C_{j,0} = q_j \frac{r_A^2}{r_s^2}, \quad (18a)$$

$$C_{j,n} = \frac{2q_j r_A J_1(\kappa_n r_A)}{\kappa_n r_s^2 J_0^2(\kappa_n r_s)} \quad (18b)$$

and the function $Q_u(r)$ can be finally written as

$$Q_u(r) = q_j \frac{r_A^2}{r_s^2} + \frac{2q_j r_A}{r_s^2} \sum_{n=1}^{\infty} \frac{J_1(\kappa_n r_A)}{\kappa_n J_0^2(\kappa_n r_s)} J_0(\kappa_n r). \quad (19)$$

The above approach is analogous to that reported by JOYCE [37] and NEWMAN [38], where it is applied to stripe-geometry edge-emitting lasers of Cartesian geometry. A similar approach was also proposed in [39] for etched-well surface-emitting lasers.

5. Solution algorithm

The $\alpha_{j,i,n}$ and $\beta_{j,i,n}$ coefficients are determined from the boundary conditions of continuity of temperature profiles and heat fluxes at all the boundaries between various layers. For temperature profiles, we obtain from Eq. (13):

$$\alpha_{j,i,0} + \beta_{j,i,0} d_i = \alpha_{j,i+1,0}, \quad (20a)$$

$$\alpha_{j,i,n} \cosh(\kappa_n d_i) + \beta_{j,i,n} \sinh(\kappa_n d_i) = \alpha_{j,i+1,n} \quad \text{for } n \geq 1, \quad (20b)$$

whereas for heat fluxes we have generally

$$k_i \beta_{j,i,0} = \begin{cases} k_{i+1} \beta_{j,i+1,0} & \text{for } i \neq j, \\ k_{i+1} \beta_{j,i+1,0} + \frac{2}{r_S^2} \int_0^{r_S} Q_j(r) r dr & \text{for } i = j, \end{cases} \quad (21a)$$

$$k_i [\alpha_{j,i,n} \sinh(\varkappa_n d_i) + \beta_{j,i,n} \cosh(\varkappa_n d_i)] = \begin{cases} k_{i+1} \beta_{j,i+1,n} & \text{for } i \neq j \text{ and } n \geq 1, \\ k_{i+1} \beta_{j,i+1,n} + \frac{2}{r_S^2 \varkappa_n^2} \int_0^{r_S} Q_j(r) J_0(\varkappa_n r) r dr & \text{for } i = j \text{ and } n \geq 1 \end{cases} \quad (21b)$$

where $Q_j(r)$ stands here for the radially dependent density of a heat flux generated at the boundary between the j -th and the $(j+1)$ -th layers. For the uniform heat source located within the $r \leq r_A$ area between the j -th and the $(j+1)$ -th layers (*cf.* Eq. (17)), Eqs. (21a) and (21b) are reduced to:

$$k_i \beta_{j,i,0} = \begin{cases} k_{i+1} \beta_{j,i+1,0} & \text{for } i \neq j, \\ k_{i+1} \beta_{j,i+1,0} + q_j \left(\frac{r_A}{r_S}\right)^2 & \text{for } i = j, \end{cases} \quad (21c)$$

$$k_i [\alpha_{j,i,n} \sinh(\varkappa_n d_i) + \beta_{j,i,n} \cosh(\varkappa_n d_i)] = \begin{cases} k_{i+1} \beta_{j,i+1,n} & \text{for } i \neq j \text{ and } n \geq 1, \\ k_{i+1} \beta_{j,i+1,n} + \frac{2q_j r_A J_1(\varkappa_n r_A)}{\varkappa_n^2 r_S^2} & \text{for } i = j \text{ and } n \geq 1 \end{cases} \quad (21d)$$

where we take advantage of Eqs. (18a) and (18b).

From the boundary conditions (12) and (11b), respectively, we have

$$\alpha_{j,1,n} = 0 \quad \text{for } n \geq 0 \quad (22)$$

and

$$\beta_{j,N,0} = 0, \quad (23a)$$

$$\alpha_{j,N,n} \sinh(\varkappa_n d_N) + \beta_{j,N,n} \cosh(\varkappa_n d_N) = 0 \quad \text{for } n \geq 1. \quad (23b)$$

Using Eq. (21a), we can write

$$\beta_{j,i,0} = \begin{cases} \frac{2}{k_i r_S^2} \int_0^{r_S} Q_j(r) r dr, & \text{for } 1 \leq i \leq j, \\ 0 & \text{for } j < i \leq N \end{cases} \quad (24a)$$

and hence, from Eq. (20a), we get

$$\alpha_{j,i,0} = \frac{2}{r_S^2} \sum_{i'=1}^{\min(i-1,j)} \frac{d_{i'}}{k_{i'}} \int_0^{r_S} Q_j(r) r dr. \quad (25a)$$

For the uniform heat source ((Eq. (17)), the above relations are reduced to:

$$\beta_{j,i,0} = \begin{cases} \frac{q_j r_A^2}{k_i r_S^2} & \text{for } 1 \leq i \leq j, \\ 0 & \text{for } j = i \leq N, \end{cases} \quad (24b)$$

$$\alpha_{j,i,0} = q_j \left(\frac{r_A}{r_S} \right)^2 \sum_{i'=1}^{\min(i-1,j)} \frac{d_{i'}}{k_{i'}}. \quad (25b)$$

We now introduce the $r_{j,i,n}$ coefficients defined as

$$r_{j,i,n} = \frac{\beta_{j,i,n}}{\alpha_{j,i,n}} \quad \text{for } i \neq 1. \quad (26)$$

Then, taking Eqs. (20b) and (21b) for $i \neq j$, we obtain

$$r_{j,i+1,n} = \frac{k_i}{k_{i+1}} \frac{\tanh(\alpha_n d_i) + r_{j,i,n}}{1 + r_{j,i,n} \tanh(\alpha_n d_i)} \quad \text{for } i \neq j \quad (27)$$

and from Eq. (23b) we have

$$r_{j,N,n} = -\tanh(\alpha_n d_N) \quad \text{for } n \geq 1. \quad (28)$$

Using again Eqs. (20b) and (21b) for $i \neq j$, but now for $i = 1$, and taking advantage of Eq. (22), we get

$$\beta_{j,1,n} = \alpha_{j,2,n} \operatorname{cosech}(\alpha_n d_1) \quad \text{for } n \geq 1 \quad (29)$$

and

$$r_{j,2,n} = \frac{k_1}{k_2} \coth(\alpha_n d_1) \quad \text{for } n \geq 1. \quad (30)$$

Now we can determine for $2 \leq i \leq N$ all $r_{j,i,n}$ working inwards from $r_{j,2,n}$ and $r_{j,N,n}$. To find all $\alpha_{j,i,n}$, we once return to Eqs. (20b) and (21b), but this time for $i = j$. After some mathematical manipulations, we have

$$\alpha_{j,j,n} = \frac{2}{\alpha_n r_S^2} \int_0^{r_S} Q_j(r) r dr [A_{j,j,n} \sinh(\alpha_n d_j) + B_{j,j,n} \cosh(\alpha_n d_j)]^{-1}, \quad \text{for } n \geq 1 \quad (31a)$$

with

$$A_{j,j,n} = k_j - k_{j+1} r_{j,j,n} r_{j,j+1,n}, \quad (32a)$$

$$B_{j,j,n} = k_j r_{j,j,n} - k_{j+1} r_{j,j+1,n}. \quad (32b)$$

Again for the uniform heat source (Eq. (17)), Eq. (31a) is reduced to

$$\alpha_{j,j,n} = \frac{2q_j r_{A,j} J_1(\kappa_n r_A)}{\kappa_n^2 r_S^2} [A_{j,j,n} \sinh(\kappa_n d_j) + B_{j,j,n} \cosh(\kappa_n d_j)]^{-1} \quad \text{for } n \geq 1. \quad (31b)$$

The remaining $\alpha_{j,i,n}$ coefficients can be determined from Eq. (20b), which after using the $r_{j,i,n}$ coefficients can be rewritten in the following form:

$$\alpha_{j,i+1,n} = \alpha_{j,i,n} [\cosh(\kappa_n d_i) + r_{j,i,n} \sinh(\kappa_n d_i)], \quad \text{for } n \geq 1. \quad (33)$$

All the $\beta_{j,i,n}$ coefficients can then be found from Eq. (26).

The full algorithm of the calculations for each heat source is therefore as follows:

1. Find $r_{j,2,n}$ from Eq. (30) for $n \geq 1$.
2. Find $r_{j,N,n}$ from Eq. (28) for $n \geq 1$.
3. Determine remaining $r_{j,i,n}$ from Eq. (27) for $n \geq 1$ and $i \geq 2$.
4. Find $\alpha_{j,j,n}$ from Eq. (31) for $n \geq 1$.
5. Determine remaining $\alpha_{j,i,n}$ from Eq. (33) for $n \geq 1$ and $i \geq 2$.
6. Determine all $\beta_{j,i,n}$ from Eq. (26) for $n \geq 1$ and $i \geq 2$.
7. Find $\beta_{j,1,n}$ from Eq. (29) for $n \geq 1$.
8. Find $\alpha_{j,1,n}$ from Eq. (22) for $n \geq 1$.
9. Find $\beta_{j,i,0}$ from Eq. (24)
10. Find $\alpha_{j,i,0}$ from Eq. (25).

6. Model convergence

Convergence of the method is illustrated in Fig. 4, where the sum of the series in Eq. (13) is plotted as a function of a number of its terms. Additionally, in Fig. 5, values of successive terms are shown. Note that in the latter case, the vertical coordinate is in a logarithmic scale.

The standard procedure is convergent very slowly. This is always the case when heat-generation areas occupy only small fraction of the whole structure [40]. With increasing numbers of terms, their values change approximately periodically, resembling the sine function but with slowly decreasing amplitude. For the centre of the active region, where the convergence process is the fastest, a ratio of the 500-th term to the sum of all 500 terms is equal to -2.8×10^{-4} and an analogous ratio for the 1000-th term equals to 9.9×10^{-5} .

To shorten the time necessary for numerical calculations, special convergence-acceleration technique is used. At first, calculations are carried out together with recording events when the series terms change their sign. After the number of sign reversals becomes equal to a declared value (usually 10 to 15), the extreme

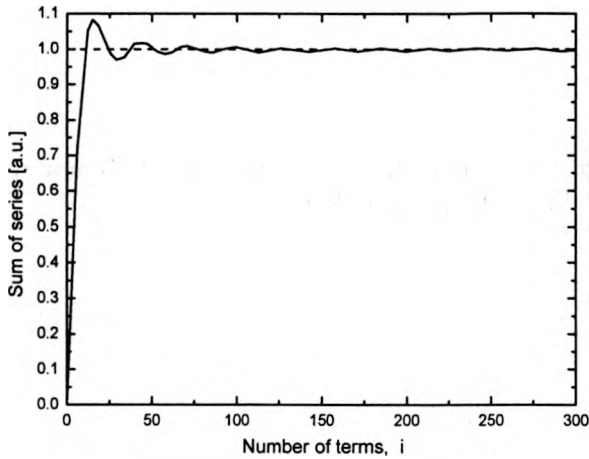


Fig. 4. Sum of the series in Eq. (13), calculated for the uniform active-region heat source, shown as a function of the number i of terms in the series.

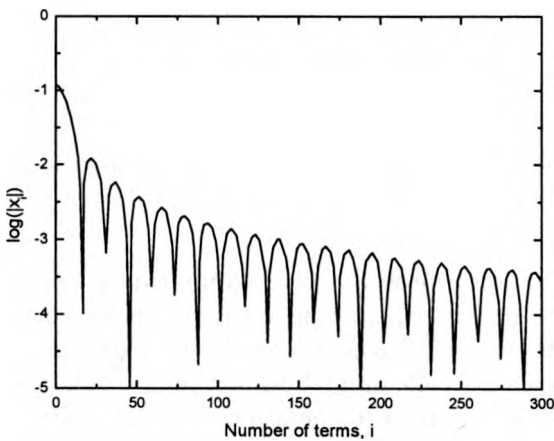


Fig. 5. Relative values of successive terms x_i in the series shown in Fig. 4, presented as a function of the term number i . The absolute value the sum of 3000 terms.

values of the series (local maxima and minima) are recorded. An arithmetic mean of four consecutive recorded extreme values of the series is taken as a result of summation.

7. Model self-consistency

In the model, thermal-electrical self-consistence of the iteration procedure is considered to be reached when the relative deviation between the active-region temperature profile obtained in two consecutive iterations $m-1$ and m , defined as

$$\sigma_m^2 = \frac{\sum_k [T_{A,m}(r_k) - T_{A,m-1}(r_k)]^2}{\sum_k T_{A,m}^2(r_k)} \quad (34)$$

is smaller than 10^{-3} . $T_{A,m}(r_k)$ in Eq. (34) denotes the temperature at the point r_k (in the active region) evaluated in the m -th iteration loop.

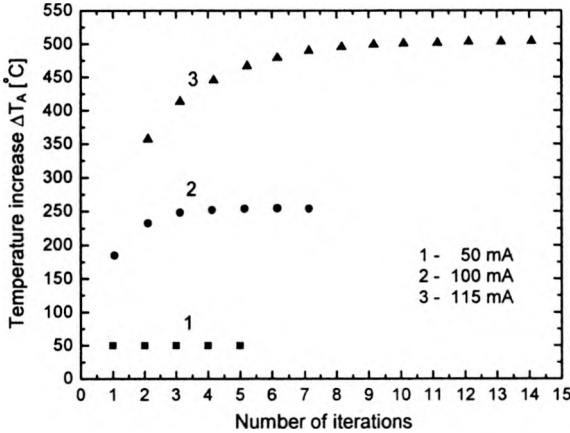


Fig. 6. Average active-region temperature increase $\Delta T_{A,av}$, calculated at the end of each iteration, shown to illustrate convergence of the self-consistent thermal-electrical iteration procedure for three values of CW pumping current.

Convergence of the self-consistent iteration procedure is exemplified in Fig. 6 for three different values of the pumping current. As one can see, very few iteration loops are necessary to reach self-consistency for relatively low excitation, just above the threshold, whereas the procedure needs much more time for high excitation level, close to thermal runaway limit. Consequently, the non self-consistent solution (the result of the first iteration) is only slightly lower than the exact solution near threshold, whereas high above threshold this difference becomes considerable.

8. Conclusions

A comprehensive analytical thermal model of proton-implanted top-surface-emitting lasers has been presented. In the model, all important heat sources have been taken into account including nonradiative recombination, reabsorption of spontaneous radiation, free-carrier absorption of laser radiation as well as volume and barrier Joule heating. Full self-consistency between thermal and electrical processes has been achieved including temperature dependence of thermal conductivities, threshold current, internal and external quantum efficiencies, voltage drop at the p-n junction, electrical resistivities and absorption coefficients. Detailed algorithm of the

model calculations is given. A special convergence-acceleration technique has been proposed. The model is applied in 24 to study some performance characteristics of typical p-side-up GaAs/AlGaAs/AlAs PITSELS operating at room temperature.

Acknowledgment – The work was supported by the Polish State Committee for Scientific Research (KBN), grants Nos. 7-T11B-069-20 and 7-T11B-073-21, and by the US-Poland Maria Skłodowska-Curie Fund No. MEN/NSF-98-336.

References

- [1] IGA K., *IEEE J. Sel. Top. Quantum Electron.* **6** (2001), 1201.
- [2] NAKWASKI W., *Opt. Quantum Electron.* **28** (1996), 335.
- [3] NAKWASKI W., OSIŃSKI M., *IEEE J. Quantum Electron.* **27** (1991), 1391.
- [4] COLDREN L. A., GEELS R. S., CORZINE S. W., SCOTT J. W., *Opt. Quantum Electron.* **24** (1992), S105.
- [5] NAKWASKI W., OSIŃSKI M., *IEEE J. Quantum Electron.* **29** (1993), 1981.
- [6] MICHALZIK R., EBELING K. J., *IEEE J. Quantum Electron.* **29** (1993), 1963.
- [7] LEE Y. H., TELL B., BROWN-GOEBELER K., JEWELL J. L., HOVE J. V., *Electron. Lett.* **26** (1990), 710.
- [8] TAI K., HASNAIN G., WYNN J. D., FISCHER R. J., WANG Y. H., WEIR B., GAMELIN J., CHO A. Y., *Electron. Lett.* **26** (1990), 1628.
- [9] LEE Y. H., JEWELL J. L., TELL B., BROWN-GOEBELER K. F., SCHERER A., HARBISON J. P., FLOREZ L. T., *Electron. Lett.* **26** (1990), 225.
- [10] TELL B., LEE Y. H., BROWN-GOEBELER K. F., JEWELL J. L., LEIBENGUTH R. E., ASOM M. T., LIVESCU G., LUTHER L., MATTERA V. D., *Appl. Phys. Lett.* **57** (1990), 1855.
- [11] LEE Y. H., TELL B., BROWN-GOEBELER K. F., JEWELL J. L., LEIBENGUTH R. E., ASOM M. T., LIVESCU G., LUTHER L., MATTERA V. D., *Electron. Lett.* **26** (1990), 1308.
- [12] CHANG-HASNAIN C. J., ORENSTEIN M., VON LEHMEN A., FLOREZ L. T., HARBISON J. P., STOFFEL N. G., *Appl. Phys. Lett.* **57** (1990), 218.
- [13] VOOK F. L., *Phys. Rev.* **135** (1964), A1742.
- [14] ZHOU P., CHENG J., SCHAUS C. F., SUN S. Z., ZHENG K., ARMOUR E., HAINS C., HSIN W., MYERS D. R., VAWTER G. A., *IEEE Photon. Techn. Lett.* **3** (1991), 591.
- [15] ZHOU P., CHENG J., SCHAUS C. F., SUN S. Z., HAINS C., ZHENG K., TORRES A., MYERS D. R., VAWTER G. A., *Appl. Phys. Lett.* **59** (1991), 2504.
- [16] TAYLOR E. W., PAXTON A. H., SCHONE H., CARSON R. F., BRISTOW J., LEHMAN J. A., HIBBS-BRENNER M. K., MORGAN R. A., MARTA T., *IEEE Trans. Nuclear Science* **45** (1997), 1514.
- [17] WOODWARD T. K., HUNSCH S., RITGER A. J., STARK J. B., *IEEE Photon. Technol. Lett.* **11** (1999), 382.
- [18] FISCHER A. J., CHOQUETTE K. D., CHOW W. W., ALLERMAN A. A., GEIB K. M., *Appl. Phys. Lett.* **77** (2000), 3319.
- [19] TAKAOKA K., ISHIKAWA M., HATAKOSHI G., [In] *17th International Semiconductor Laser Conference*, September 25–28, 2000, p. 93.
- [20] TANSU N., ZHOU D., RUSLI S., MAWST L. J., [In] *12th IEEE Lasers and Electro-Optics Society Annual Meeting*, LEOS'99, San Francisco, November 8–11, 1999, Vol. 2, p. 397.
- [21] STARCK C., BOUCART J., PLAIS A., BOUCHE N., DEROUIN E., PINQUIER A., GABORIT F., BONNET-GAMARD J., FORTIN C., GOLDSTEIN L., BRILLOUET F., SALET P., CARPENTIER D., MARTINEAU M.-F., JACQUET J., *Conference on Lasers and Electro-Optics*, CLEO'99, May 23–25, 1999, p. 454.
- [22] KAZIMIERSKI C., DEBRAY J. P., MADANI R., SAGNES J., OUGAZZADEN A., BOUADMA N., ETRILLARD J., ALEXANDRE F., QUILLEC M., *Electron. Lett.* **35** (1999), 811.
- [23] MAĆKOWIAK P., SARZAŁA R. P., NAKWASKI W., *International Workshop on Nitride Semiconductors*, IWN'2000, Nagoya, Japan, September 24–27, 2000, Proceedings, IPAP Conference Series 1 (2000), 889.

- [24] NAKWASKI W., MAĆKOWIAK P., OSIŃSKI M., *Opt. Appl.* **32** (2002), 173.
- [25] ZHOU P., CHENG J., SCHAUS C.F., SUN S.Z., ZHENG K., ARMOUR E., HAINS C., HSIN W., MYERS D.R., VAWTER G.A., *IEEE Photon. Technol. Lett.* **3** (1991), 591.
- [26] ETTENBERG M., SOMMERS H.S., Jr., KRESSEL H., LOCKWOOD H.F., *Appl. Phys. Lett.* **18** (1971), 571.
- [27] WEBER J.-P., *Propagation of light in periodic structures: Application to the surface-emitting laser diodes fabricated by phase-locked epitaxy*, Ph.D. dissertation, University of California at Berkeley, 1990.
- [28] JENSEN S. M., BARNOSKI M.K., HUNSPERGER R.G., KAMATH G.S., *J. Appl. Phys.* **46** (1975), 3547.
- [29] MERZ J.L., LOGAN R.A., SERGENT A.M., *J. Appl. Phys.* **47** (1976), 1436.
- [30] TSANG W.T., *IEEE J. Quantum Electron.* **20** (1984), 1119.
- [31] SPITZER W.G., WHELAN J.M., *Phys. Rev.* **114** (1959), 59.
- [32] CHAND N., FISCHER R., KLEM J., HENDERSON T., PEARAH P., MASSELINK W.T., CHANG Y.C., MORKOÇ H., *J. Vac. Sci. Technol. B* **3** (1985), 644.
- [33] SWAMINATHAN V., ZILKO J.L., TSANG W.T., WAGNER W.R., *J. Appl. Phys.* **53** (1982), 5163.
- [34] KUCHARSKA A.I., ROBBINS D. J., *IEEE J. Quantum Electron.* **26** (1990), 443.
- [35] NAKWASKI W., OSIŃSKI M., CHENG J., *Appl. Phys. Lett.* **61** (1992), 3101.
- [36] SPIEGEL M.R., *Theory and Problems of Advanced Mathematics for Engineers and Scientists*, McGraw-Hill, New York 1971.
- [37] JOYCE W.B., DIXON R.W., *J. Appl. Phys.* **46** (1975), 855.
- [38] NEWMAN D.H., BOND D.J., STEFANI J., *Solid-State Electron Dev.* **2** (1978), 41.
- [39] IGA K., KOYAMA F., *Surface Emitting Lasers (Ohm-sha)*, Chap. 2.2, 1990.
- [40] LEE C.C., PALISOC A.L., *IEEE Trans. Components, Hybrids, Manuf. Technol.* **11** (1988), 485.

Received March 18, 2002